MOVING TOWARDS A-PRIORI IDENTIFICATION OF UNDESIRABLE PILOT BIOMETRICS FOR COLLECTIVE BOUNCE INSTABILITY

Andrea Zanoni
andrea.zanoni@polimi.it
Post Doc
Politecnico di Milano
Milano, Italy

Vincenzo Muscarello
vincenzo.muscarello@polimi.it
Post Doc
Politecnico di Milano
Milano, Italy

Abstract

The interaction between the helicopter vibrations and the pilot involuntary control input, filtered through the biomechanical response of the pilot's body, can lead to the emergence of adverse, possibly even unstable, feedback loops, which in turn produce a degradation of the vehicle handling qualities. These phenomena are called Pilot-Assisted Oscillations (PAO). One of the most important is the "Collective Bounce", caused by vertical vibrations of the cockpit inducing an unwanted collective control input. On the rotorcraft side, the main rotor coning mode excitation has been shown to produce a phase margin reduction in the collective pitch-heave loop transfer function. On the pilot's side, biometrics such as stature, weight, age and sex are known to play a major role, but relatively limited effort has been placed in exploring the effects of their variability. especially exploiting predictive numerical techniques in a virtual engineering framework. This work represents a first attempt at filling the gap. A detailed multibody model of the pilot's upper body , featuring the full musculoskeletal biomechanics of the upper limbs and a simplified, Component Mode Synthesis representation of the torso, is coupled with a simplified rotorcraft model. that reproduces the vertical dynamics of the vehicle, including the coning mode response. A pseudo-random population of pilots, exhibiting different biometrics, is generated and the corresponding multibody biomechanical models are derived. The population is then simulated in a feedback loop with the rotorcraft dynamics and allowed to evolve, through a genetic (de-)optimization algorithm, towards the individuals most likely to be prone to instability. The result of the (de-)optimization process is the identification of the worst possible pilot biometrics with regard to collective bounce proneness on the modeled rotorcraft.

1 INTRODUCTION

The interaction of the pilot with the helicopter dynamics is characterized not only by voluntary activity, which is intended to produce the control inputs required to perform a specific task, but also by involuntary actions. The latter is the result of the unintentional application of controls caused by vibrations of the cockpit. Such vibratory motion is filter by the pilot's biomechanical characteristics and may produce involuntary control inputs through the so called biodynamic feedthrough (BDFT[1]). Pilot's involuntary commands may further excite the dynamics of the vehicle, causing a degradation of the flight dynamics qualities, difficulties in achieving the desired performance and may ultimately produce an unstable closure of the control feedback loop[2;3;4]. This problem, widely known as Pilot-Assisted Oscillation (PAO), may affect all kind of aircraft whose pilot is accommodated within the vehicle and is thus subjected to its motion. Usually, PAO-related control inputs are characterized by frequencies between 2 – 8 Hz[5]; thus, in PAO events the interaction is with the aeroelastic modes of the vehicle. For this range of frequencies the pilot is no longer capable of intentionally producing commands to compensate for the undesired motion, while at higher frequencies the biomechanical response of the human body is expected to filter out any excitation originating from the motion of the cockpit.

PAO phenomena have been extensively analyzed in fixed-wing aircraft, primarily only when they have been unexpectedly encountered in flight. The situation is similar for rotary-wing aircraft, although the number of reported events and studies is, in comparison, rather limited: one notable exception is represented by the work of Walden[6].

Walden[6] presented and extensive discussion of aeromechanical instabilities that occurred on several rotorcraft during their development and acceptance by the U.S. Navy, including the CH-46, UH-60, SH-60, CH-53, V-22, and AH-1. Most of those events involved the involuntary participation of the pilot interacting with the automatic flight control system (AFCS).

Generally, any attempt to reduce the vehicle's PAO tendency was conducted on a case-by-case basis, and it was usually addressed by procedural mitigations. Planned structural interventions were either deferred or canceled due to the lack of time or resources.

One of the most important PAO phenomena in helicopters is the so-called "Collective Bounce", caused by vertical vibrations of the cockpit. As a consequence of the most common cockpit and control inceptors layout, the vibrations induce a collective control input as a result of the biodynamics of the pilot's left arm. This, in turn, excites the vertical vibrations by directly inducing a change in rotor thrust along the vertical axis. In[7], Gennaretti et al. discussed occurrences of this phenomenon and investigated it numerically, identifying the influencing factors and the modeling requirements for its simulation. A closed-loop aeroelastic experiment involving the collective bounce was presented and discussed by Masarati et al. in[8]. In[9] Muscarello et al. pinpointed the phase margin reduction introduced by the main rotor coning mode in the collective pitch–heave loop transfer function as the key factor in the manifestation of collective bounce.

The investigation of PAO instabilities requires the capability to model aeroservoelastic phenomena as well as the dynamic behavior of the pilot. A simplified helicopter model, able to capture the collective bounce dynamics in hover, has been proposed in[9]. It consists of the vertical motion of the entire helicopter and the rotor coning motion. The pilot's BDFT can be modeled as a set of mechanical impedances between the motion of the seat and the resulting actuation of the control inceptors, since no voluntary action can be envisaged. Experimental results obtained so far have shown how pilot's arms response to vibrations is characterized by an high level of variability[10;11]. As a consequence it should be considered as an highly uncertain element in the dynamic modeling of this kind of problems. The variability of the pilot involuntary action, filtered through the dynamical characteristics of the human body, is at the root of the uncertainty. Thus, to answer the question: "which is the most collective-bounce prone pilot?" it is necessary to move towards the answer moving from first-principle basis: the multibody approach has proven to be very beneficial to this end, allowing to generate a virtual model of the pilot biomechanical response starting from its anthropometric data[12;13].

In order to assess the effects of the variability of the anthropometric data on the performance parameters with respect to PAO phenomena, a fully numerical procedure has been developed. It consists in several steps:

- a set of pseudo-random anthropometric parameters is generated;
- the corresponding multibody model is built;
- the multibody model is simulated in order to identify the pilot's BDFT between the seat vertical acceleration and the collective lever rotation;
- the resulting state space pilot model is simulated in a feedback loop with the simplified helicopter model, in order to evaluate the figures of (de-)merit with respect to PAO resilience.

A genetic (de-)optimization algorithm has been developed to identify the set of biometric parameters that are associated with the most instability-prone pilots: each pilot is treated as an individual of a population, encoding his anthropometric characteristics into a genome. Based on this set of parameters, a complete upper body biomechanical multibody model of the pilot is generated and its interaction with the simplified helicopter model evaluated to yield a figure of (de-)merit inversely proportional to the stability margins of the pilot-vehicle system (PVS). Individuals among the population are then assigned a *fitness* inversely proportional to said margins, such as to allow the *worst* pilots the best probability to breed. The algorithm ultimately yields the *worst* possible combinations of anthropometric parameters for a particular rotorcraft.

2 BDFT IDENTIFICATION

The human upper body dynamics has long been recognized as a critical component involved in PAO phenomena [2]. To account for varying pilot body types, the multibody approach has been adopted from the authors' research group at Politecnico di Milano since 2012 [14] and developed ever since.

Several steps are needed to estimate the pilot's BDFT with respect to the heave axis of a helicopter. The general procedure will be outlined briefly, since it is described in detail in several previous publications [15;16]. The novel parts will be evidenced and explained in a more exhaustive way.

Generally, to identify the linearized biodynamic behavior of the pilot it is necessary to

- define the reference mission task elements that delineate the control context;
- generate a set of geometrical and inertial parameters from the pilot biometrics and the corresponding multibody model of the upper limbs (and torso);
- identify, through an inverse kinematics analysis, the reference configuration of the upper body;
- calculate the reference muscle lengths and activation patterns solving an inverse dynamics problem: since the system is overactuated, an optimization problem needs to be solved;
- perform a direct dynamics analysis, yielding the pilot control input as a function of the vehicle's vertical acceleration input;
- analyze the output of the direct analysis to identify the transfer function between the vertical acceleration and the collective inceptor rotation.

The reference mission chosen for the analysis is a Position Task (PT) [17], requiring the pilot to apply and maintain 50% of the collective input. It is a kind of task that needs precise control, resulting in a more *stiff* neuromuscular behavior.

2.1 The multibody model

Over the last several years, a detailed biomechanical multibody model of the pilot's body has been developed at the Department of Aerospace Science and Technology (DAST) of Politecnico di Milano: it is implemented in the general-purpose, free software MBDyn[1], also internally developed at DAST. It features the full representation of the pilot upper limbs, each one possessing 7 degrees of freedom and actuated by a set of 25 Hill-type, one dimensional muscle actuators [14;15;18]. The upper limbs model has been coupled with a Component Mode Synthesis (CMS) model of the human torso to complete the description of the pilot's upper body dynamics.

In the current form, the biomechanical multibody model of the pilot is cast into a modular architecture: it can be used to predict the dynamics of the complete upper body, i.e. both limbs comprising the shoulder girdles and the torso [13;12] or be reduced to exclude portions that are not considered relevant in the analysis of interest. For the present work, a simplified model comprising the left an right upper limb, excluding the shoulder girdles, has been used. The model was originally developed following the work of Pennestr et al. [19].

The single limb (Cfr. Fig. 1) comprehends rigid bodies representing the humerus, the radius, the ulna and the hand. The latter is considered as a single rigid body, since it is involved only in grasping tasks. The total number of degrees of freedom of a single limb is thus $4 \cdot 6 = 24$. Ideal algebraic constraints connect the rigid bodies representing the bones and the corresponding muscle masses. The humerus is connected to the torso through a spherical joint, situated in the functional center of the humerus proximal epicondyle. The radius is connected to the humerus through a spherical joint as well, situated in the functional center of the humerus distal epicondyle. The ulna is connected to the humerus by means of a revolute hinge, whose axis of rotation lies close to perpendicular to the mechanical longitudinal axis of the ulna and passes through the center of the throclea. The deviation from perfect perpendicularity of the two axes is the so-called *carrying angle*, i.e. the angle formed between the arm and the forearm mechanical axes. In this work, a 8 carrying angle for male subjects and a 10 carrying angle for female subjects have been selected. The ulna and the radius are connected by an *in line* joint, that constraints a point offset medially from the radius to move along the mechanical axis of the ulna. The offset is such as the two bones lie parallel when the arm is extended anteriorly with the

[1] http://www.mbdyn.org

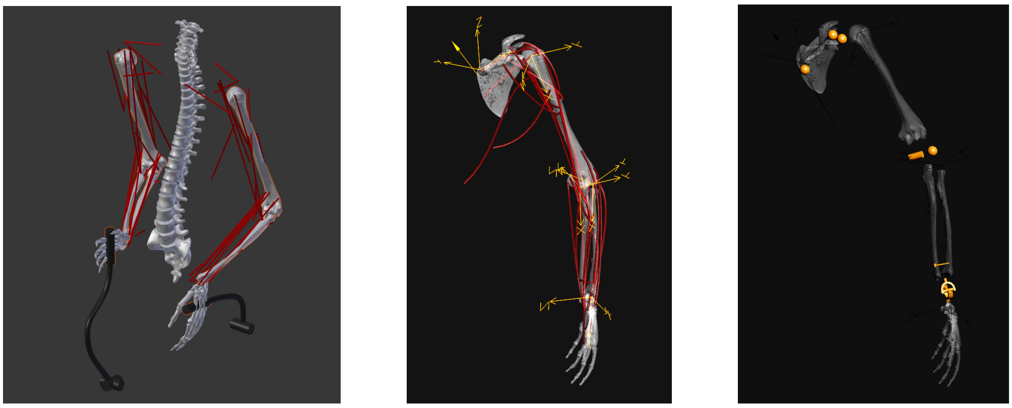

(a) (b) (c)

Figure 1: The biomechanical multibody model of the upper limbs and torso.

palm facing upward. The hand is connected to the radius by a Cardano joint, allowing only the flexion-extension and the medial-lateral rotations. The total number of degrees of freedom is thus $24-3-3-5-2-4=7$, meaning that the single limb is a kinematically underconstrained system even when the 6 degrees of freedom of the hand are prescribed.

2.2 Solution phases

To assess the variability of the bioservoelastic interaction between the pilot and the vehicle with respect to the pilot's body characteristics, it is of crucial importance to be able to represent, as realistically as possible, a wide variety of pilots with possibly very different anthropometric parameters. To this end, the upper limbs model has been extended with a specific set of procedures to generate its geometrical, inertial and muscular properties[13] based on a set of standard anthropometric data: stature, weight, age and sex. The model is fully parametrized and can be adapted starting from reference scaling parameters for the ribcage, obtained from data published by Shi et al.[20]. Inertial parameters are scaled based on regression models found in[21;22;23;24;25].

The model is assembled in the standard anatomical position. To bring it to the reference configuration for subsequent dynamical analysis, an inverse kinematics analysis has to be performed first. The single upper limb, as noted above, is a kinematically underdetermined system when all six degrees of freedom of the hand are imposed, having a total of 7 degrees of freedom. To work around the problem, a procedure involving the direct solution of the kinematics at the position level has been developed, based on a previous work by Masarati et al.[26;14;15]: an equivalent static system, constrained by nonlinear elastic elements representing *ergonomic* penalty functions is solved at each timestep. The resulting configuration is transferred as the initial configuration of the inverse and direct dynamic analyses.

To be able to estimate the muscular activation patterns in a given reference configuration, is it necessary to estimate the joint torques through the solution of an inverse dynamics problem and subsequently estimate the force that each muscle bundle should introduce. 25 total muscle fascicula are modeled in each limb, represented by monodimensional viscoelastic elements that can be actuated. The force in the single muscle is a function of the current length and elongation velocity of the muscle, as well as the current voluntary activation state a through a relationship simplifying a Hill-type muscle, originally proposed by Pennestr et al. in[19]:

$$f_i(x,v,a)=F_0\left(f_1(x_i)f_2(v_i)\cdot a_i+f_3(x_i)\right), \quad (1)$$

where F_0 is the reference peak isometric contraction force, x the nondimensional length of the muscle with respect to the isometric length, $x=l/l_0$, v the reference contraction velocity $v=\dot{l}/l_0$ and a the activation parameter, with $0\le a_i\le 1$. The reference activation is computed minimizing the activation of the muscles, $\min_{a_i}\sum_i a_i^2$, constrained by the aforementioned bounds on a_i. It is a function not only of the geometrical configuration of the cockpit but also of the collective lever inertial properties.

The reference model configuration in terms of both kinematics and muscular activation is thus reached and a direct dynamics analysis can now be performed, perturbing the system around such state. In this phase, to model the voluntary (albeit passive) contribution of the muscular activation to the reference value found in the inverse dynamics phase, a *reflexive* contribution is added, through a quasi-steady approximation, as discussed in[15;18;16], based on previous work made by Stroeve[27], namely:

$$a_i = a_{i,0} - K_p \left(x_i - x_{i,0} \right) - K_d v_i. \tag{2}$$

The process here outlined yields a model of a virtual pilot, ready to undergo a virtual test in order to identify the transfer function between the collective control input and the vertical acceleration of the vehicle. In previous works, the identification process has been carried out through (virtual) testing of the model response to single-harmonic or band-pass filtered random excitation in the range 1-10 Hz[12;16]. This kind of analyses are however, very time consuming and thus do not allow for a wide range statistical exploration of the dependence of the collective bounce (and in general PAO) proneness of the pilot-vehicle system (PVS). Therefore, an alternative approach based on the eigenanalysis of the multibody model about the reference configuration has been developed.

2.3 Direct Eigenanalysis

MBDyn directly solves a DAE problem in the form

$$\mathbf{M}\dot{\mathbf{x}} = \mathbf{p}, \tag{3}$$
$$\dot{\mathbf{p}} + \mathbf{\Gamma}^T_{/\mathbf{x}}\boldsymbol{\lambda} = \mathbf{f}(\dot{\mathbf{x}}, \mathbf{x}, t), \tag{4}$$
$$\mathbf{\Gamma}(\mathbf{x}) = \mathbf{0}, \tag{5}$$

in which $\mathbf{x}$ is the vector of the nodes' generalized coordinates, $\mathbf{p}$ the vector of their momenta, $\mathbf{\Gamma}(\mathbf{x})$ collects the joints' algebraic relationships, $\boldsymbol{\lambda}$ the Lagrange multipliers and $\mathbf{f}$ the external loads. By collecting $\mathbf{y}^T = \left[\mathbf{x}^T, \mathbf{p}^T, \boldsymbol{\lambda}^T\right]^T$ the problem can be cast into the implicit form, with appropriate initial conditions

$$\mathbf{g}(\dot{\mathbf{y}}, \mathbf{y}, t) = \mathbf{0}, \tag{6a}$$
$$\mathbf{y}(t_0) = \mathbf{y}_0. \tag{6b}$$

The perturbation of the implicit DAEs system is

$$\mathbf{g}_{/\mathbf{y}}\delta\mathbf{y} + \mathbf{g}_{/\dot{\mathbf{y}}}\delta\dot{\mathbf{y}} = -\mathbf{g}. \tag{7}$$

MBDyn integrates in time the equations (6) through multi-step, predictor-corrector methods. In the prediction step, an estimate of the solution at time step k is formed according to the solution at l previous time steps

$$\mathbf{y}_k = \sum_{i=1}^{l} a_i \mathbf{y}_{k-i} + h \sum_{j=0}^{l} b_j \dot{\mathbf{y}}_{k-j} \tag{8}$$

where h is the time step. Perturbing the last equation yields

$$\delta\mathbf{y}_k = h b_0 \delta\dot{\mathbf{y}}_k \tag{9}$$

inserting the relationship (9) into equation (7) yields a purely algebraic problem

$$\left(\mathbf{g}_{/\dot{\mathbf{y}}} + h b_0 \mathbf{g}_{/\mathbf{y}}\right)\delta\dot{\mathbf{y}} = -\mathbf{g} \tag{10}$$

In fact, MBDyn actually computes the Jacobian Matrix of this Newton step as

$$\mathbf{J}(c) = \mathbf{g}_{/\dot{\mathbf{y}}} + c\mathbf{g}_{/\mathbf{y}}, \tag{11}$$

so that matrices $\mathbf{g}_{\dot{\mathbf{y}}}$ and $\mathbf{g}_{/\mathbf{y}}$ are never explicitly available. As discussed in[28], the eigenanalysis of the model can be then posed on matrices $\mathbf{J}(c)$ and $\mathbf{J}(-c)$, rewriting the problem as

$$\left(\Lambda_k \mathbf{J}(c) + \mathbf{J}(-c)\right)\mathbf{Y}_{Rk} = \mathbf{0}, \tag{12}$$

where equilibrium is assumed, i.e. the right hand term in eq. (7) is considered null.

This is required for the eigenanalysis to make sense, but not strictly enforced in MBDyn, which leaves the responsibility of selecting the appropriate system configuration about which to linearize to the user.

$$\Lambda_k = \frac{1 + c\lambda_k}{1 - c\lambda_k} \tag{13}$$

that can be inverted to yield the *real* eigenvalues

The *real* eigenvalues of the system are then computed as

$$\lambda_k = \frac{1}{c}\frac{\Lambda_k - 1}{\Lambda_k + 1}. \tag{14}$$

Matrices $\mathbf{g}_{\dot{\mathbf{y}}}$ and $\mathbf{g}_{/\mathbf{y}}$ can ultimately be recovered through a simple manipulation

$$\mathbf{g}_{/\dot{\mathbf{y}}} = \frac{\mathbf{J}(c) + \mathbf{J}(-c)}{2}, \quad \mathbf{g}_{/\mathbf{y}} = \frac{\mathbf{J}(c) - \mathbf{J}(-c)}{2c}. \tag{15}$$

2.4 State space model

Projecting matrices $\mathbf{g}_{/\dot{\mathbf{y}}}$ and $\mathbf{g}_{/\mathbf{y}}$ onto a subspace of the left and right eigenvector spaces, respectively spanned by $\tilde{\mathbf{Y}}_L$ and $\tilde{\mathbf{Y}}_R$, yields a state-space representation of the linearized dynamics of the original system

(16) $$\tilde{\mathbf{Y}}_L \mathbf{g}_{/\dot{\mathbf{y}}} \tilde{\mathbf{Y}}_R \delta\dot{\mathbf{q}} + \tilde{\mathbf{Y}}_L \mathbf{g}_{/\mathbf{y}} \tilde{\mathbf{Y}}_R \delta\mathbf{q} = \mathbf{0},$$

where the space of generalized coordinates perturbations is linearly mapped to the space of modal coordinates perturbations, namely

(17) $$\delta\mathbf{y} = \tilde{\mathbf{Y}}_R \delta\mathbf{q}.$$

Considering now the output $\mathbf{w}$ as a linear function of the state variables perturbations

(18) $$\mathbf{w} = \tilde{\mathbf{C}} \delta\mathbf{y},$$

so that the complete state-space representation of the system's dynamics is written in descriptor form

(19) $$\mathbf{E}\delta\dot{\mathbf{q}} = \mathbf{A}\delta\mathbf{q},$$
(20) $$\mathbf{w} = \mathbf{C}\delta\mathbf{q},$$

having defined

(21) $$\mathbf{E} = \tilde{\mathbf{Y}}_L \mathbf{g}_{/\dot{\mathbf{y}}} \tilde{\mathbf{Y}}_R, \qquad \mathbf{B} = \mathbf{0},$$
(22) $$\mathbf{A} = -\tilde{\mathbf{Y}}_L \mathbf{g}_{/\mathbf{y}} \tilde{\mathbf{Y}}_R, \qquad \mathbf{C} = \tilde{\mathbf{C}}\tilde{\mathbf{Y}}_R.$$

In projecting the problem onto the subspace spanned by the reduced modal coordinates $\mathbf{q}$, care has to be taken in selecting a subset of the generalized eigenvectors as to avoid those related to the static behavior of the system, constrained kinematic variables, and Lagrange multipliers[29]. In practical terms, only eigenvectors whose associated eigenvalues are not infinite or zero are retained. This choice leads to an invertible $\mathbf{E}$ matrix.

2.5 Input due to imposed motion

In the present case, the system input is due to the seat vertical motion. This means that vector $\delta\mathbf{y}$ of equation can be split into two a *free* part $\delta\mathbf{y}^F$ and an *imposed* part $\delta\mathbf{y}^I$:

(23) $$\delta\mathbf{y} = \begin{Bmatrix} \delta\mathbf{y}^F \\ \delta\mathbf{y}^I \end{Bmatrix},$$

the imposed part of $\delta\mathbf{y}$ is represented by generalized coordinates expressing the vertical translation of the seat and the corresponding velocity. Matrices $\mathbf{g}_{/\dot{\mathbf{y}}}$ and $\mathbf{g}_{/\mathbf{y}}$ can be partitioned accordingly. E.g. for $\mathbf{g}_{/\mathbf{y}}$:

(24) $$\mathbf{g}_{/\mathbf{y}} = \begin{bmatrix} \mathbf{g}_{/\mathbf{y}}^{FF} & \mathbf{g}_{/\mathbf{y}}^{FI} \\ \mathbf{g}_{/\mathbf{y}}^{IF} & \mathbf{g}_{/\mathbf{y}}^{II} \end{bmatrix}.$$

The rightmost block column of the resulting system can be brought to the right hand side of eq. (7), as it pertains to the forcing terms due to the imposed motion

(25) $$\mathbf{g}_{/\dot{\mathbf{y}}}^{FF} \delta\dot{\mathbf{y}}^F + \mathbf{g}_{/\mathbf{y}}^{FF} \delta\mathbf{y}^F = -\mathbf{g}_{/\dot{\mathbf{y}}}^{FI} \delta\dot{\mathbf{y}}^I - \mathbf{g}_{/\mathbf{y}}^{FI} \delta\mathbf{y}^I.$$

The descriptor form state space representation of the system in now defined by the matrices

(26) $$\overline{\mathbf{E}} = \tilde{\mathbf{Y}}_L^{FF} \mathbf{g}_{/\dot{\mathbf{y}}}^{FF} \tilde{\mathbf{Y}}_R^{FF}$$
(27) $$\overline{\mathbf{B}} = -\tilde{\mathbf{Y}}_L^{FF} \mathbf{g}_{/\dot{\mathbf{y}}}^{FI} - \tilde{\mathbf{Y}}_L^{FF} \mathbf{g}_{/\mathbf{y}}^{FI} = \overline{\mathbf{B}}_1 + \overline{\mathbf{B}}_2$$
(28) $$\overline{\mathbf{A}} = -\tilde{\mathbf{Y}}_L^{FF} \mathbf{g}_{/\mathbf{y}}^{FF} \tilde{\mathbf{Y}}_R^{FF}$$
(29) $$\overline{\mathbf{C}} = \tilde{\mathbf{C}} \tilde{\mathbf{Y}}_R^{FF},$$

where $\tilde{\mathbf{C}}$ is particularly simple in its structure, since the system's only output, the collective control rotation ϕ, is a single component of $\delta\mathbf{y}$. The transfer function between the vertical acceleration of the seat and the collective control rotation can now be computed directly by considering the system's behavior in the Laplace domain

(30) $$\begin{aligned} \left(s\overline{\mathbf{E}} - \overline{\mathbf{A}}\right) \delta\mathbf{Y}^{FF}(s) &= \left(s\overline{\mathbf{B}}_1 + \overline{\mathbf{B}}_2\right) \delta\mathbf{Y}^I(s), \\ \mathbf{w}(s) &= \overline{\mathbf{C}} \delta\mathbf{Y}^{FF}(s), \end{aligned}$$

that yields

(31) $$H_{BDFT}(s) = \frac{1}{s^2} \cdot \overline{\mathbf{C}} \left(s\overline{\mathbf{E}} - \overline{\mathbf{A}}\right)^{-1} \left(s\overline{\mathbf{B}}_1 + \overline{\mathbf{B}}_2\right),$$

where the double integrator $1/s^2$ has been added to consider the relationship between the vertical acceleration of the pilot's seat $\ddot{z}$ and the collective inceptor rotation ϕ. However, it gives an integrator-like low-frequency asymptotic behavior, $1/s$, that is not physical (a pilot would always be able to compensate the error corresponding to a slow enough input) and overlaps with the pilot's voluntary behavior[9]. The low-frequency asymptotic behavior can be corrected by adding a second-order high-pass filter with cutoff frequency ω_h slightly above the crossover frequency ω_c of the voluntary pilot's model.

This procedure leads to a considerable reduction of the time needed to estimate the pilot's BDFT: while the numerical experiment technique time requirement is in the order of minutes, both for the single harmonic excitation and the band-limited noise input, the time required by the eigenanalysis-based procedure is in the order of seconds, typically significantly less than 10". Thus, a broad exploration of the space of the pilots biometrics is now a viable option, that has been exploited by evaluating the stability of a combined PVS model into a genetic algorithm searching for the most *undesirable* pilot biometrics.

3 HELICOPTER MODEL

In hover, rotors respond to changes in the blade collective pitch with collective flap motion. This motion is called the rotor blade coning motion, and it is described by the collective flap angle β_0. The basics of rotor blade flapping coupled with helicopter vertical motion in hover are briefly reviewed in this section. The objective is to use the equations of motion that characterize only the helicopter dynamics that may be relevant for the involuntary interaction with the pilot during the collective bounce phenomenon.

3.1 Simplified analytical model

The simplified helicopter model used for preliminary vertical bounce investigations consists of the vertical motion of the entire helicopter and the rotor coning mode[9], as shown in Fig. 2.

The helicopter model is drastically simplified, since it neglects the details of the rotor hub geometry and kinematics, the drive train dynamics and many details of basic rotor aerodynamics like inflow, twist, tip loss, etc., that may be significant in performance analysis but are considered inessential for the desired perturbative model, or require not easily accessible information. Since the work focuses on perturbation in hover along the vertical axis, only the collective (i.e. uniform with respect to azimuth) term of the kinematic parameters is considered, yielding a set of linear time invariant (LTI) equations:

(32a)
$$m\ddot{z}+n_b\frac{\gamma}{4}\Omega\frac{I_\beta}{R^2}\dot{z}+n_bS_\beta\ddot{\beta}+n_b\frac{\gamma}{6}\Omega\frac{I_\beta}{R}\dot{\beta} = n_b\frac{\gamma}{6}\Omega^2\frac{I_\beta}{R}\vartheta,$$

(32b)
$$n_bI_\beta\ddot{\beta}+n_b\frac{\gamma}{8}\Omega I_\beta\dot{\beta}+n_bI_\beta\nu_\beta^2\Omega^2\beta+n_bS_\beta\ddot{z}+n_b\frac{\gamma}{6}\Omega\frac{I_\beta}{R}\dot{z} = n_b\frac{\gamma}{8}\Omega^2 I_\beta\vartheta,$$

where the symbols are defined in Table 1 with the data of the IAR 330 Puma helicopter (see Ref.[9]) here used as benchmark model.

Table 1: IAR 330 Puma: Simplified model data

IAR 330 Puma	Symbol	Value	Units
Total mass	m	7345.00	kg
Number of blades	n_b	4	n.d.
Rotor radius	R	7.49	m
Rotation speed	Ω	4.50	Hz
Lock number	γ	8.70	n.d.
Flap static moment	S_β	276.48	kg m
Flap inertia moment	I_β	1339.19	kg m^2
Flap frequency ratio	ν_β	1.03	n.d.

Eq. 32a describes the vertical displacement of the helicopter and Eq. 32b describes the rotor coning. Coupling occurs thanks to inertia forces, by way of the static moment S_β of the blades, and to aerodynamics by way of the change in angle of attack related to the vertical velocity of the aircraft, $\dot{z}$, and to the blade flapping rate $\dot{\beta}$. In the following, the simplified helicopter model is essentially seen as a Single Input/Single Output (SISO) system in the Laplace domain in the form:

(33)
$$\ddot{z}\left(s\right) = H_{\ddot{z}\vartheta}\left(s\right)\vartheta\left(s\right).$$

3.2 Collective control inceptor

The collective control inceptor, sketched in Fig. 2(b), usually provides minimal force feedback; thus no force other than that exerted by the pilot contrasts the motion of the lever when the pilot command it. However, to improve the quality of its positioning and in the end the "touch and feel" of the pilot, some force threshold needs to be overcome in order to move the lever from the rest. In helicopters controlled by direct mechanical transmission of the command, this effect is produced by some artificial friction that resists the motion of the lever. The minimum amount of friction is usually prescribed by the manufacturer and the actual amount can be adjusted to best suit the pilot's needs.

In the present analysis, friction acting on the collective lever rotation is not directly considered, since it is hard to deal with in linear frequency domain models; the stick–slip effect associated with transition from pure adhesion to sliding and vice versa is omitted. All these simplifications are considered conservatives. The motion of the collective control inceptor prescribes the collective pitch angle of the rotor blades. In augmented control helicopters, the motion of the control is the collective pitch demand to actuators, either directly or through a Flight Control System (FCS). In usual arrangements, the full range $\Delta\phi$ of the control

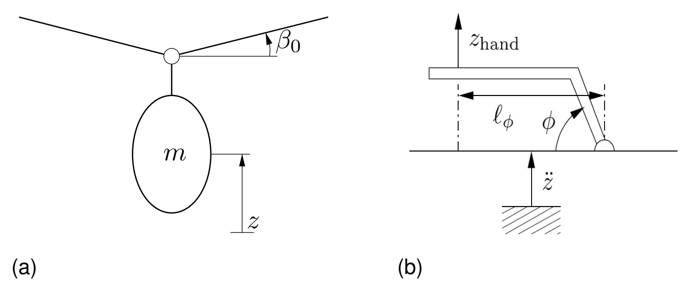

Figure 2: Simplified helicopter model (a) and sketch of collective control inceptor (b).

lever rotation ranges from 35 to 45 degrees for a lever length l_ϕ of about 270 to 350 mm from the hinge to the hand grip. An estimation of the gear ratio between the control lever rotation and the collective pitch rotation can be obtained as:

$$\vartheta = \frac{\Delta\vartheta}{\Delta\phi} \cdot \phi, \tag{34}$$

The collective pitch range, $\Delta\vartheta$, is of the order of 20 degrees. The parameters l_ϕ and $\Delta\phi$ depend on the cockpit layout while the parameter $\Delta\vartheta$ may depend on the rotor design; in augmented control designs it may even vary in flight according to some scheduling.

3.3 Loop closure on the vertical axis

The loop is closed by feeding the pilot-control device BDFT to the simplified helicopter model through the appropriate gear ratio between the collective pitch rotation and the collective lever rotation, equal to $G_0 = \Delta\vartheta/\Delta\phi$ = 1.1 rad/m on the proposed IAR 330 Puma model. The collective lever might also consider an additional input ϕ' (e.g. due to the voluntary pilot action) added to the pilot's BDFT contribution, which yields

$$\phi = H_{BDFT}(s)\,\ddot{z} + \phi', \tag{35}$$

fed into the helicopter TF of Eq. 33 through the collective pitch gear ratio,

$$(1 - G_0 H_{BDFT}(s)\, H_{\ddot{z}\vartheta}(s))\,\ddot{z} = G_0 H_{\ddot{z}\vartheta}(s)\,\phi'. \tag{36}$$

The Loop Transfer Function (LTF) is thus the coefficient of $\ddot{z}$ in Eq. (36) minus 1, namely:

$$H_{LTF}(s) = -G_0 H_{BDFT}(s)\, H_{\ddot{z}\vartheta}(s). \tag{37}$$

With the proposed SISO analytical model it is possible to investigate the stability of the PVS. Instead of using the classical eigenvalues investigation, it is possible to exploit the robust stability analysis approach, obtaining information about the grade of stability with respect to parameter variations [30;31;32]. The Nyquist criterion is very explicative because it intuitively expresses the stability degree of robustness as the distance of each point of the LTF frequency response from the point $(-1 + \mathrm{j}0)$ in the Argand diagram (see chapter 7 of Ref. [33]). Robust stability indices are phase (P_M) and gain (G_M) margins. The phase margin is the phase difference between the crossing of the LTF with the unit circle and -180 deg., namely $180 - \angle H_{LTF}\left(\mathrm{j}\omega_{|H_{LTF}|=1}\right)$. The gain margin is $1/H_{LTF}\left(\mathrm{j}\omega_{(-180)}\right)$, i.e. the inverse of the LTF magnitude at ω corresponding to -180 deg of phase. Positive margins indicate a stable system, while to obtain robust systems is usually necessary to reach gain margins above 6 dB and phase margins of 60 deg.

4 GENETIC (DE-)OPTIMIZATION ALGORITHM

As mentioned in the previous sections, the significant reduction in simulation time needed to estimate the pilot's BDFT, combined with the possibility offered by the multibody approach to easily generate a consistent model representing a broad variety of pilot's body types, make it possible to explore in a statistical meaningful sense the space of the pilot biometrics. In order to do so, a genetic algorithm has been set up to search for the pilot's biometrics that produce the minimum values of P_M and G_M. The (de-)optimization problem is actually an unconstrained, bounded minimization problem on P_M and G_M that can be stated as follows:

$$\min J = G_M(\mathbf{x}_b) + P_M(\mathbf{x}_b) \quad \text{s.t.} \quad \mathbf{x}_{b,l} \le \mathbf{x}_b \le \mathbf{x}_{b,u} \tag{38}$$

i.e. find the anthropometric parameters $\mathbf{x}_b$ that minimize the stability margins of the PVS, subjected to upper and lower bounds on the parameters. Vector $\mathbf{x}_b$ has three components that depend on the type of analysis: most commonly, age a, weight w and stature h of the pilot. An alternative choice, that will be exploited in the following sections, is the use of the Body Mass Index $BMI = w/h^2$, to limit the population of pilots to more realistic body types.

Finally, $\mathbf{x}_b$ contains the parameters of Mayo-like feedthrough transfer functions capturing the involuntary, linearized behavior of the pilot.

An initial population of N pilots is generated as a pseudo-random Sobol set. Each individual of the population is characterized by the vector $\mathbf{x}_{b,i}$, that can be considered its *genome*. The objective function J_i is evaluated for each individual and the population is sorted to assign to each individual a *fitness* inversely proportional to its *ranking* as a non-dominated element of the set of all the possible combinations of parameters values, as suggested by Goldberg[34]. The individuals with the greatest fitness are selected for crossover (the generation of the new offspring) via a *roulette wheel* strategy[35], i.e. by assigning to each individual a range of values between 0 and 1, the amplitude of which is proportional to their fitness, and then generating a random number, also among 0 and 1. The single individual is selected if the generated number falls in its interval.

The result of the crossover stage is an offspring of N individuals. Among the total of $2N$ individuals, the most fit N are selected and retained in the next iteration of the algorithm. The cycle stops when at least 90% of the total individuals have ranking 1, i.e. are on the Pareto Optimal front, or the maximum number of allowed iterations has been reached.

5 Results

5.1 Parameter exploration of Mayo Transfer Function

Mayo[36] identified a simple model for BDFT of a human body to describe the involuntary action of helicopter pilots on the collective control inceptors when subjected to vertical vibration of the cockpit. In particular, Mayo identified the TFs between the absolute vertical acceleration of the pilot hand, $\ddot{z}_{h.abs}$, as a function of the vertical acceleration of the vehicle, $\ddot{z}$. As discussed in[9], these TFs need to be written as the relative acceleration of the hand, $\ddot{z}_{hand}$, with respect to the vehicle acceleration, and integrated two times to regain a low-frequency correct behavior, resulting in

$$\ddot{z}_{hand} = \ddot{z}_{h.abs} - \ddot{z} = -s\frac{s + 1/\tau_p}{s^2 + 2\xi_p\omega_p s + \omega_p^2}\ddot{z}. \quad (39)$$

Two set of pilots have been investigated by Mayo, called ectomorphic (small and lean build) and mesomorphic (large bone structure and muscle build). The structural properties of the Mayo's ectomorphic and mesomorphic TFs are reported in Ref.[36]. It should be remembered that the TF of Eq. (39) must be integrated twice to yield the relative displacement of the hand, $z_{hand} = \ddot{z}_{hand}/s^2$. However, the double integration gives an integrator-like low-frequency asymptotic behavior, $1/s$, that is not physical (a pilot would always be able to compensate the error corresponding to a slow enough input) and overlaps with the pilot's voluntary behavior[9]. The low-frequency asymptotic behavior can be corrected by adding a second-order high-pass filter with cutoff frequency ω_h slightly above the crossover frequency ω_c of the voluntary pilot's model. Since ω_c is less than 0.5 Hz, while the pilot's biomechanical poles are at about 3.5 Hz, the bands of interest of the pilot's voluntary and involuntary models should be adequately separated. The combination of the double integration and high-pass filtering yields

$$H_{BDFT}(s) = -\frac{1}{l_\phi}\frac{s}{(s+\omega_h)^2}\frac{s + 1/\tau_p}{s^2 + 2\xi_p\omega_p s + \omega_p^2}, \quad (40)$$

where a numerical value of ω_h = 3.10 rad/s has been used in Eq. (40). The control lever length has been also added in Eq.40 in order to convert the vertical displacement of the lever, i.e. z_{hand}, in collective lever rotations ϕ.

Table 2: Structural properties of Mayo's TFs.

Ectomorphic Pilot	Symbol	Value	Units
Frequency	ω_p	3.380	Hz
Damping ratio	ξ_p	32.000	%
Time constant	τ_p	0.117	sec
Mesomorphic Pilot	Symbol	Value	Units
Frequency	ω_p	3.750	Hz
Damping ratio	ξ_p	28.000	%
Time constant	τ_p	0.107	sec

A first application of the (de-)optimization algorithm has been conducted on the LTF with the Mayo's identified BDFT in feedback loop with the IAR 330 Puma simplified helicopter model. The main parameters of the pilot's TFs have been changed between the following lower/upper boundaries: the time constant, τ_p, ranges from 60 to 120 ms, the damping ratio, ξ_p, ranges from 20 to 50 % and the pilot's biomechanical frequency, ω_p, between 2.5 and 4.0 Hz.

Results are reported in Fig. 3. The final population, representing the worst case scenario (i.e. the pilot's BDFT returning the smallest gain and phase margins), is characterized by the pilots with the smallest damping ratios (as expected) and the smallest natural biomechanical frequencies. The natural frequency mainly impacts on the static gain of the pilot's BDFT. The lower is the natural frequency, the higher will be the static gain of the pilot's BDFT, thus acting on the LTF robust stability decreasing the gain margin. Also the time constant may have an impact on the pilot's static gain, although the algorithm has founded an higher sensitivity to the natural frequency, confirming that the time constant mainly acts to restore the correct pilot phase behavior to the higher frequencies.

Unfortunately, limiting the analysis to the information contained in the Mayo's TFs, it is not possible to recover the pilot's anthropometric characteristics related to the *worst* pilot body type. These information can, however, be obtained by the biomechanical multibody model of the pilot's body.

As described in section 2.1, the upper body biomechanical multibody model can tailored on a specific set of anthropometric parameters and analyzed to yield the corresponding pilot BDFT transfer function with respect to the collective bounce. The genetic (de-)optimization algorithm has been applied using the input parameters reported, along with their bounds, in Table 3. The population size is 100 individuals, and the probability of mutation 10%. The algorithm stopped after 30 iterations, performed in approximately 8.5 hours.

Table 3: Parameters for pilot biometrics exploration: in this case, the weight and the stature of the pilot was let vary independently. LB and UB stand for Lower Bound and Upper Bound.

Parameter	Symbol	LB	UB	Units
Age	a	25	65	years
Weight	w	60	110	kg
Stature	h	1550	2000	mm

In Fig. 4, the results of the application of the algorithm of section 4 with the parameters shown in Table 3 are shown. The population seems to evolve towards individuals with the largest Body Mass Index (BMI). In fact, the average individual in the final population has a stature around 1.6 m and a body mass close to 110 kg, resulting in a BMI of about 42. This value corresponds to severely obese individuals and it is thus very unlikely to be found in real pilots. Thus, a second run has been performed, this time using the BMI as an input parameter instead of directly considering the weight.

Table 4: Parameters for pilot biometrics exploration: in this case, the weight and the stature of the pilot was let vary independently.

Parameter	Symbol	LB	UB	Units
Age	a	25	65	years
Body Mass Index	BMI	18	30	kg m^{-2}
Stature	h	1550	2000	mm

In Fig. 5 the results of the aforementioned second run, considering pilots with BMI limited to more plausible values (Cfr. Table 4), are shown. The lower and upper bounds for BMI, respectively 18 and 30, have been chosen as to limit the population to individuals in the normal and overweight range, excluding underweight and obese body types. In this case the algorithm stopped after 30 iterations, converging towards individuals with greater BMI, height and age, as shown in Figure 5(b). Generally, body types with higher BMI are associated with a lower biomechanical natural frequency[36]. The natural frequency mainly impacts on the static gain of the pilot's BDFT. The lower is the natural frequency, the higher will be the static gain of the pilot's BDFT, thus acting on the LTF robust stability decreasing the gain margin.

A possible explanation for the different results regarding the height of the most problematic body types, with respect to the previous run, is that the BMI has greater influence with respect to the other parameters, and the global minimum of the objective function is located in a region of the parameter space that the algorithm could not explore in the second run, as it was outside of the problem's bounds.

In order to try to identify the solution, Analysis of Variance (ANOVA) techniques are being implemented at the time of writing of this manuscript: variations of the stability figures of merit will be tested against variations of the parameters of both the helicopter model and the pilot biomechanical model in order to identify the most relevant actors

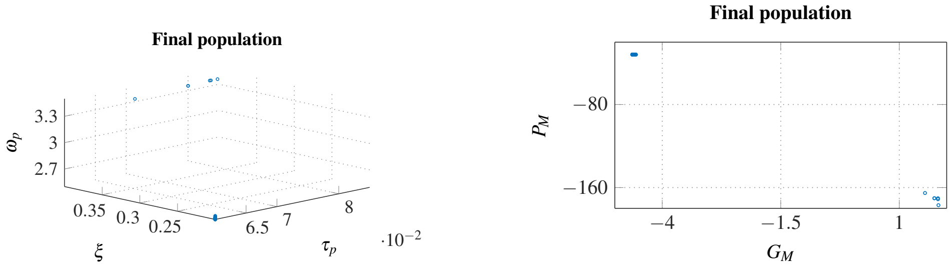

(a) (b)

Figure 3: Results of the Mayo's pilot parameter exploration conducted with the genetic algorithm described in section 4.

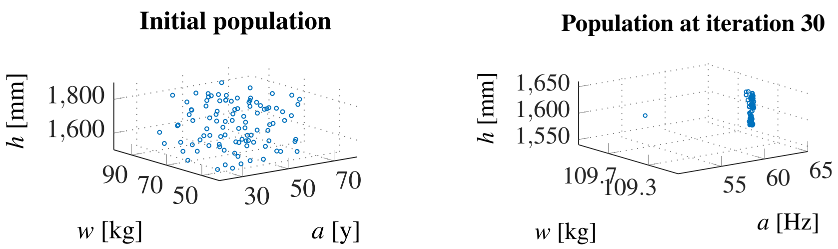

(a) (b) (c)

Figure 4: Results of the pilot biometric exploration conducted with the genetic algorithm outlined at section 4. In (a), the initial population is shown. The final population after 30 iterations, is shown in (b). In (c) the identified Pareto front is shown.

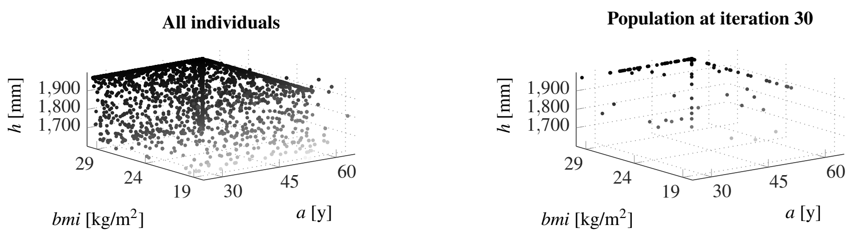

(a) (b)

Figure 5: Results of the pilot biometric exploration conducted with the genetic algorithm outlined at section 4. In (b), the population at the last iteration is shown. In (a), all the individual generated in each iteration are shown. Darker color of the markers corresponds to a more collective bounce prone body type.

and the possible correlations amongst them. The results of this latter analysis are postponed to future publications.

6 CONCLUSIONS

This work presents a novel approach to identify the pilot anthropometric characteristics that make the closed-loop pilot-rotorcraft system specifically prone to the collective bounce phenomenon. The parameters for pilots biometrics exploration are the age, weight, stature or alternatively the Body Mass Index (BMI). A pseudo-random population of pilots, exhibiting different biometrics, is generated and the corresponding multibody biomechanical models are derived. The population is then simulated in a feedback loop with the rotorcraft dynamics and allowed to evolve, through a genetic (de-)optimization algorithm, towards the individuals most likely to be prone to instability. Results shown that the population seems to evolve towards individuals with heavy weight, around 110 kg, and short stature, i.e. 1.6 m, resulting in huge, unrealistic, BMI values of about 42. Consequently a second run has been performed using the BMI as an input parameter instead of directly considering the weight. The lower and upper BMI bounds were set to 18–30. In this case the algorithm converges towards individuals with greater BMI, height and age, showing that the BMI has a greater influence with respect to the other parameters. Future developments will consider Analysis of Variance (ANOVA) techniques in order to identify the most relevant actors between the pilot biometrics and the rotorcraft parameters and the possible correlations amongst them.

References

[1] Henry R. Jex and Raymond E. Magdaleno. Biomechanical models for vibration feedthrough to hands and head for a semisupine pilot. *Aviation, Space, and Environmental Medicine*, 49(1–2):304–316, 1978.

[2] Marilena D. Pavel, Michael Jump, Binh Dang-Vu, Pierangelo Masarati, Massimo Gennaretti, Achim Ionita, Larisa Zaichik, Hafid Smaili, Giuseppe Quaranta, Deniz Yilmaz, Michael Jones, Jacopo Serafini, and Jacek Malecki. Adverse rotorcraft pilot couplings — past, present and future challenges. *Progress in Aerospace Sciences*, 62:1–51, October 2013. doi:10.1016/j.paerosci.2013.04.003.

[3] Marilena D. Pavel, Pierangelo Masarati, Massimo Gennaretti, Michael Jump, Larisa Zaichik, Binh Dang-Vu, Linghai Lu, Deniz Yilmaz, Giuseppe Quaranta, Achim Ionita, and Jacopo Serafini. Practices to identify and preclude adverse aircraft-and-rotorcraft-pilot couplings — a design perspective. *Progress in Aerospace Sciences*, 76:55–89, 2015. doi:10.1016/j.paerosci.2015.05.002.

[4] D. T. McRuer. *Aviation Safety and Pilot Control: Understanding and Preventing Unfavourable Pilot-Vehicle Interactions*. Washington DC: National Research Council, National Academy Press, 1997.

[5] O. Dieterich, J. Götz, B. DangVu, H. Haverdings, P. Masarati, M. D. Pavel, M. Jump, and M. Gennaretti. Adverse rotorcraft-pilot coupling: Recent research activities in Europe. In *34th European Rotorcraft Forum*, Liverpool, UK, September 16–19 2008.

[6] R. Barry Walden. A retrospective survey of pilot-structural coupling instabilities in naval rotorcraft. In *American Helicopter Society 63rd Annual Forum*, pages 1783–1800, Virginia Beach, VA, May 1–3 2007.

[7] Massimo Gennaretti, Jacopo Serafini, Pierangelo Masarati, and Giuseppe Quaranta. Effects of biodynamic feedthrough in rotorcraft-pilot coupling: Collective bounce case. *J. of Guidance, Control, and Dynamics*, 36(6):1709–1721, 2013. doi:10.2514/1.61355.

[8] Pierangelo Masarati, Giuseppe Quaranta, Linghai Lu, and Michael Jump. A closed loop experiment of collective bounce aeroelastic rotorcraft-pilot coupling. *Journal of Sound and Vibration*, 333(1):307–325, January 2014. doi:10.1016/j.jsv.2013.09.020.

[9] Vincenzo Muscarello, Giuseppe Quaranta, and Pierangelo Masarati. The role of rotor coning in helicopter proneness to collective bounce. *Aerospace Science and Technology*, 36:103–113, July 2014. doi:10.1016/j.ast.2014.04.006.

[10] M. Jump, S. Hodge, B. DangVu, P. Masarati, G. Quaranta, M. Mattaboni, M. D. Pavel, and O. Dieterich. Adverse rotorcraft-pilot coupling: Test campaign development at the university of Liverpool. In *34th European Rotorcraft Forum*, Liverpool, UK, September 16–19 2008.

[11] M. Mattaboni, G. Quaranta, P. Masarati, and M. Jump. Experimental identification of rotorcraft pilots' biodynamic response for investigation of PAO events. In *35th European Rotorcraft Forum*, pages 1–12, Hamburg, Germany, September 22–25 2009.

[12] Pierangelo Masarati, Giuseppe Quaranta, and Andrea Zanoni. A detailed biomechanical pilot model for multi-axis involuntary rotorcraft-pilot couplings. In *41st European Rotorcraft Forum*, Munich, Germany, September 1–4 2015.

[13] A. Zanoni and P. Masarati. Geometry generation and benchmarking of a complete multibody model of the upper limb. In *4th Joint International Conference on Multibody System Dynamics*, Montreal, Canada, May 29–June 2 2016.

[14] Andrea Zanoni, Pierangelo Masarati, and Giuseppe Quaranta. Upper limb mechanical impedance variability estimation by inverse dynamics and torque-less activation modes. In P. Eberhard and P. Ziegler, editors, *2nd Joint International Conference on Multibody System Dynamics*, Stuttgart, Germany, May 29–June 1 2012.

[15] Pierangelo Masarati, Giuseppe Quaranta, and Andrea Zanoni. Dependence of helicopter pilots' biodynamic feedthrough on upper limbs' muscular activation patterns.

Proc. IMechE Part K: J. Multi-body Dynamics, 227(4):344–362, December 2013. doi:10.1177/1464419313490680.

[16] Pierangelo Masarati, Giuseppe Quaranta, Andrea Bernardini, and Giorgio Guglieri. A multibody model for piloted helicopter flight dynamics and aeroservoelasticity. *J. of Guidance, Control, and Dynamics*, 38(3):431–441, 2015. doi:10.2514/1.G000837.

[17] J. Venrooij, D. A. Abbink, M. Mulder, M. M. van Paassen, and M. Mulder. Biodynamic feedthrough is task dependent. In *2010 IEEE International Conference on Systems Man and Cybernetics (SMC)*, pages 2571–2578, Istanbul, Turkey, October 10–13 2010. doi:10.1109/ICSMC.2010.5641915.

[18] Pierangelo Masarati and Giuseppe Quaranta. Bioaeroservoelastic analysis of involuntary rotorcraft-pilot interaction. *J. of Computational and Nonlinear Dynamics*, 9(3):031009, July 2014. doi:10.1115/1.4025354.

[19] E. Pennestrì, R. Stefanelli, P. P. Valentini, and L. Vita. Virtual musculo-skeletal model for the biomechanical analysis of the upper limb. *Journal of Biomechanics*, 40(6):1350–1361, 2007. doi:10.1016/j.jbiomech.2006.05.013.

[20] X. Shi, L. Cao, M Reed, J. Rupp, C. Hoff, C. Hoff, and J. Hu. A statistical human rib cage geometry model account for variations by age, sex, stature and body mass index. *Journal of Biomechanics*, 47:2277–2285, 2014.

[21] R.F. Chandler, C.E. Clauser, J.T. McConville, H.M. Reynolds, and J.W. Young. Investigation of inertial properties of the human body. TR DOT ES-801 430, DOT - NHTSA, 1975.

[22] John T McConville, Charles E Clauser, Thomas D Churchill, Jaime Cuzzi, and Ints Kaleps. Anthropometric relationships of body and body segment moments of inertia. Technical report, DTIC Document, 1980.

[23] R. Dumas, L. Chèze, and J-P. Verriest. Adjustments to mcconville et al. and young et al. body segment inertial parameters. *Journal of Biomechanics*, 40(3):543 – 553, 2007.

[24] James Cheverud, Claire C. Gordon, Robert A. Walker, Cashell Jacquish, Luci Kohn, Allen Moore, and Nyuta Yamashita. 1988 anthropometric survey of US Army personnel: correlation coefficients and regression equations. part 1: Statistical techniques, landmark, and mesurement definitions. TR 90/032, NATICK, 1990.

[25] James Cheverud, Claire C. Gordon, Robert A. Walker, Cashell Jacquish, Luci Kohn, Allen Moore, and Nyuta Yamashita. 1988 anthropometric survey of US Army personnel: correlation coefficients and regression equations. part 4: Bivariate regression tables. TR 90/035, NATICK, 1990.

[26] Alessandro Fumagalli, Gabriella Gaias, and Pierangelo Masarati. A simple approach to kinematic inversion of redundant mechanisms. In *ASME IDETC/CIE 2007*, Las Vegas, Nevada, 4–7 September 2007. (DETC2007-35285).

[27] Sybert Stroeve. Impedance characteristics of a neuromusculoskeletal model of the human arm II. movement control. *Biological Cybernetics*, 81(5–6):495–504, 1999. doi:10.1007/s004220050578.

[28] P. Masarati. Direct eigenanalysis of constrained system dynamics. *Proc. IMechE Part K: J. Multi-body Dynamics*, 223(4):335–342, 2009. doi:10.1243/14644193JMBD211.

[29] Matteo Ripepi and Pierangelo Masarati. Reduced order models using generalized eigenanalysis. *Proc. IMech. E Part K: J. Multi-body Dynamics*, 225:1–14, 2011. doi:10.1177/14644193JMBD254.

[30] Giuseppe Quaranta, Vincenzo Muscarello, and Pierangelo Masarati. Lead-lag damper robustness analysis for helicopter ground resonance. *J. of Guidance, Control, and Dynamics*, 36(4):1150–1161, July 2013. doi:10.2514/1.57188.

[31] Giuseppe Quaranta, Aykut Tamer, Vincenzo Muscarello, Pierangelo Masarati, Massimo Gennaretti, Jacopo Serafini, and Marco Molica Colella. Rotorcraft aeroelastic stability using robust analysis. *CEAS Aeronaut. J.*, 5(1):29–39, March 2014. doi:10.1007/s13272-013-0082-z.

[32] Vincenzo Muscarello, Pierangelo Masarati, and Giuseppe Quaranta. Robust stability

analysis of adverse aeroelastic roll/lateral rotorcraftpilot couplings. *Journal of the American Helicopter Society*, 62(2):1–13, 2017.

[33] Sigurd Skogestad and Ian Postlethwaite. *Multivariable Feedback Control*. John Wiley & Sons, Chichester, 2005.

[34] D.E. Goldberg. *Genetic Algorithms in Search, Optimization, and Machine Learning*. Artificial Intelligence. Addison-Wesley Publishing Company, Boston, 1989.

[35] Giampiero Mastinu, Massimiliano Gobbi, and Carlo Miano. *Optimal Design of Complex Mechanical Systems*, volume 1. Springer-Verlag, Berlin, Deutschland, 2006.

[36] John R. Mayo. The involuntary participation of a human pilot in a helicopter collective control loop. In *15th European Rotorcraft Forum*, pages 81.1–12, Amsterdam, The Netherlands, 12–15 September 1989.